MOLECULAR AND CELLULAR BIOLOGY, July 2002, p. 5212–5221 Vol. 22, No. 14
0270-7306/02/$04.00+0 DOI: 10.1128/MCB.22.14.5212–5221.2002

Targeted Deletion of Both Thymidine Phosphorylase and Uridine Phosphorylase and Consequent Disorders in Mice

Misako Haraguchi,[1] Hiroaki Tsujimoto,[2] Masakazu Fukushima,[2] Itsuro Higuchi,[3] Hideto Kuribayashi,[4] Hideo Utsumi,[4] Atsuo Nakayama,[5] Yoshio Hashizume,[6] Junko Hirato,[7] Hiroki Yoshida,[8] Hiromitsu Hara,[8] Shinjiro Hamano,[9] Hiroaki Kawaguchi,[10] Tatsuhiko Furukawa,[1] Kohei Miyazono,[11] Fuyuki Ishikawa,[12] Hideo Toyoshima,[13] Tadashi Kaname,[14] Masaharu Komatsu,[1] Zhe-Sheng Chen,[1] Takenari Gotanda,[1] Tokushi Tachiwada,[1] Tomoyuki Sumizawa,[1] Kazutaka Miyadera,[2] Mitsuhiro Osame,[3] Hiroki Yoshida,[10] Tetsuo Noda,[15] Yuji Yamada,[2] and Shin-ichi Akiyama[1]*

Department of Cancer Chemotherapy, Institute for Cancer Research,[1] Third Department of Internal Medicine,[3] and Department of Pathology,[10] Faculty of Medicine, Kagoshima University, Kagoshima 890-8520, Hanno Research Center, Taiho Pharmaceutical Co., Ltd., Hanno, Saitama,[2] Department of Biophysics, Graduate School of Pharmaceutical Sciences,[4] Department of Immunology, Medical Institute of Bioregulation,[8] and Department of Parasitology, Graduate School of Medical Sciences,[9] Kyushu University, Fukuoka 812-8582, Department of Pathology, Nagoya University School of Medicine, Showa-ku, Nagoya 466-8550,[5] Institute for Medical Science of Aging, Aichi Medical University, Aichi-gun, Aichi 480-1195,[6] First Department of Pathology, Gunnma University School of Medicine, Maebashi 371-8511,[7] Department of Biochemistry[11] and Department of Cell Biology,[15] The Cancer Institute of Japanese Foundation for Cancer Research, Tokyo 170-8455, Graduate School of Bioscience and Biotechnology, Tokyo Institute of Technology, Yokohama,[12] Department of Internal Medicine, Institute of Clinical Medicine, University of Tsukuba, Tsukuba 305,[13] and Department of Developmental Genetics, Institute of Molecular Embryology and Genetics, Kumamoto University School of Medicine, Kumamoto,[14] Japan

Received 11 March 2002/Accepted 26 March 2002

Thymidine phosphorylase (TP) regulates intracellular and plasma thymidine levels. TP deficiency is hypothesized to (i) increase levels of thymidine in plasma, (ii) lead to mitochondrial DNA alterations, and (iii) cause mitochondrial neurogastrointestinal encephalomyopathy (MNGIE). In order to elucidate the physiological roles of TP, we generated mice deficient in the *TP* gene. Although TP activity in the liver was inhibited in these mice, it was fully maintained in the small intestine. Murine uridine phosphorylase (UP), unlike human UP, cleaves thymidine, as well as uridine. We therefore generated TP-UP double-knockout ($TP^{-/-}$ $UP^{-/-}$) mice. TP activities were inhibited in $TP^{-/-}$ $UP^{-/-}$ mice, and the level of thymidine in the plasma of $TP^{-/-}$ $UP^{-/-}$ mice was higher than for $TP^{-/-}$ mice. Unexpectedly, we could not observe alterations of mitochondrial DNA or pathological changes in the muscles of the $TP^{-/-}$ $UP^{-/-}$ mice, even when these mice were fed thymidine for 7 months. However, we did find hyperintense lesions on magnetic resonance T_2 maps in the brain and axonal edema by electron microscopic study of the brain in $TP^{-/-}$ $UP^{-/-}$ mice. These findings suggested that the inhibition of TP activity caused the elevation of pyrimidine levels in plasma and consequent axonal swelling in the brains of mice. Since lesions in the brain do not appear to be due to mitochondrial alterations and pathological changes in the muscle were not found, this model will provide further insights into the causes of MNGIE.

In most mammalian cells, there are two different pyrimidine nucleoside phosphorylases, uridine phosphorylase (UP) (EC 2.4.2.3) and thymidine phosphorylase (TP) (EC 2.4.2.4), which catalyze the reversible conversion of pyrimidine (deoxy)riboside to pyrimidine base and (deoxy)ribose-1-phosphate. The substrate specificity of mouse UP is different from that of human UP. Human UP cleaves uridine but not thymidine or deoxyuridine. Mouse UP cleaves both thymidine and uridine (5). Fukushima et al. reported that phosphorolysis of the thymidine analogue, 5-trifluoromethyl-2′-deoxyuridine (F_3dThd) in mouse liver but not mouse small intestine was inhibited by the TP inhibitor that specifically inhibits TP activity. They therefore suggested that phosphorolysis of F_3dThd in the mouse small intestine is catalyzed mainly by UP (7).

In cancer patients and tumor-bearing animals, the level of TP in plasma is elevated (26), and its expression in various solid tumors is higher than in the adjacent nonneoplastic tissues (23, 33, 37). In 1992, we demonstrated that TP is identical to platelet-derived endothelial cell growth factor (18, 32, 35; T. Furukawa, A. Yoshimura, T. Sumizawa, M. Haraguchi, S. Akiyama, K. Fukui, M. Ishizawa, and Y. Yamada, Letter, Nature **356:**668, 1992). Both TP itself and the degradation product of thymidine, 2-deoxy-D-ribose, had chemotactic and angiogenic activities (1, 15, 19, 30; M. Haraguchi, K. Miyadera, K. Uemura, T. Sumizawa, T. Furukawa, K. Yamada, S. Akiyama, and Y. Yamada, Letter, Nature **368:**198, 1994), and the enzymatic activity of TP was required for its angiogenic activity (17). TP was expressed mainly at the invasive edges of tumors (28), and TP expres-

* Corresponding author. Mailing address: Institute for Cancer Research, Faculty of Medicine, Kagoshima University, 8-35-1 Sakuragaoka, Kagoshima 890-8520, Japan. Phone: 81-992-75-5490. Fax: 81-992-65-9687. E-mail: akiyamas@m3.kufm.kagoshima-u.ac.jp.

sion was associated with the extent of invasion of gastric and colorectal carcinoma (28, 34).

Mitochondrial neurogastrointestinal encephalomyopathy (MNGIE) is a unique autosomal-recessive disorder exhibiting mitochondrial DNA (mtDNA) alterations. The disease is characterized clinically by ptosis, progressive external ophthalmoparesis, gastrointestinal dysmotility, cachexia, peripheral neuropathy, and leukoencephalopathy. Muscle biopsies typically revealed ragged-red fibers and focal cytochrome *c* oxidase (COX) deficiency (2, 11, 24). Nishino et al. mapped the disease locus and identified *TP* as the causative gene. TP activity in peripheral leukocytes of 15 MNGIE patients was severely reduced. These authors therefore concluded that the loss-of-function mutations in the *TP* gene led to an increase in the thymidine level in plasma, causing mtDNA abnormalities and MNGIE (12, 20–22).

To assess the physiological functions of TP and to ascertain whether the pathogenic mechanism of MNGIE is related to aberrant thymidine metabolism, we generated mice deficient in the *TP* gene. $TP^{-/-}$ mice are apparently normal, and neither pathological nor biological features of MNGIE were observed for up to 21 months after birth. We noted that TP activity in the small intestine was retained in $TP^{-/-}$ mice. We therefore generated mice lacking both *TP* and *UP* genes in order to completely inhibit the TP activity. $TP^{-/-}$ $UP^{-/-}$ mice appear to be healthy and survive for up to 16 months, suggesting that other factors might contribute to MNGIE pathology. Mutations in *SCO2*, a COX assembly gene located on chromosome 22, have recently been reported in patients with fetal infantile cardioencephalomyopathy associated with severe COX deficiency in heart and skeletal muscle. The SCO2 protein is thought to function as a copper chaperone in the assembly of COX subunits I and II (4, 16, 25, 31). Nishino et al. performed genetic linkage study to find *TP* as the candidate of causative gene for MNGIE (20). We found that the mouse *TP* gene overlaps with the *SCO2* gene and that the human *TP* gene (exon 10) is located next to the *SCO2* gene. Although COX activity was not decreased in $TP^{-/-}$ $UP^{-/-}$ mice, magnetic resonance imaging (MRI) abnormalities in the cerebra were consistently found in these mice. Ultrastructural observation revealed that the myelin sheaths of the enlarged fibers in $TP^{-/-}$ $UP^{-/-}$ mice have segmental dilatation in the tangential view and uneven protrusion in the transverse view. This mouse model provided new insights into the histological basis of the MRI abnormalities. Furthermore, we found alteration in the pharmacokinetics of administered drugs in $TP^{-/-}$ and $TP^{-/-}$ $UP^{-/-}$ mice. This model is useful for elucidating the extent of involvement of the *TP* gene in the features of MNGIE and for predicting the efficacy of medical treatment for MNGIE patients who have lost TP activity.

MATERIALS AND METHODS

Generation of mice with a targeted deletion in TP. Genomic clones encoding fragments of the murine *TP* gene were obtained from the Mouse ES BAC Genomic Library (INCYTE, St. Louis, Mo.) by screening it with the full-length human *TP* cDNA as a probe. Two overlapping BAC clones spanning the full-length murine *TP* gene were identified. An 11.5-kb *Spe*I-*Spe*I fragment of the clone containing all exons of the *TP* gene was inserted into the pGEM5Z vector. A targeting vector was designed by replacing a 1.6-kb genomic TP fragment that included the sequence coding for the phosphate- or deoxyribose-binding site with a neomycin resistance cassette. A diphtheria toxin A cassette was blunt-end ligated into the 5′ end of the targeting construct. The targeting vector was linearized with *Aat*II and electroporated into embryonic stem (ES) cells from 129/svJ mice. After selection with G418, homologous recombinants were identified by Southern blotting according to standard protocols. Clones heterozygous for the targeted mutation were injected into C57BL/Swiss blastocytes to generate chimeric mice. Chimeric mice were crossed into C57BL/Swiss strains to produce heterozygous mutant mice. Germ line transmission of the mutation was verified by PCR analysis of tail DNA. The presence of the wild-type allele and the disrupted allele was determined by allele-specific PCR analysis. The primer upstream of the disruption site, GAGCGCTGTAACCCGACCCT (oligonucleotide TPf), and the primer downstream of the disruption site, TATCACCGCG TGCACGAAGTTTC (oligonucleotide TPr), were used for amplification of the wild-type allele. The sequence of the primer derived from the *neo* gene was CCGATTCGCAGCGCATCGCC (oligonucleotide Neo). Oligonucleotides TPf and Neo were used for generation of the knockout allele.

The use of animals in this research complied with all relevant guidelines of the Japanese government and Kagoshima University.

Generation of mice with targeted deletions of both TP and UP. $TP^{-/-}$ mice were crossed with $UP^{+/-}$ mice to generate $TP^{+/-}$ $UP^{+/-}$ mice. These mice were subsequently intercrossed to generate $TP^{-/-}$ $UP^{-/-}$ mice. Mice were routinely genotyped by PCR analysis of tail DNA.

The primers for UP were UPG2 (CAAAGCTGAGGCCCAACTGCCATGG) and UPG3 (CCTTGGACTTCCATTCACAGCTGCG) for the wild-type allele and PGK3 (CCTGAAGAACGAGATCAGCAGCCTC) and UPG4 (AGCTCT TGCTCCTTCGCCTGCTTGC) for the mutant allele.

Enzyme assays. TP activity was assayed by measuring the conversion of [^{14}C]thymidine to [^{14}C]thymine as described previously (6). TP activity was expressed as nanomoles of thymidine catalyzed to thymine per minute per milligram of protein.

Determination of the plasma concentration of pyrimidine nucleoside. Five mice at 5 weeks of age were sacrificed and exsanguinated, and the blood was centrifuged to obtain plasma. The levels of thymidine, uridine, and cytidine were measured as described previously (7).

Determination of the concentration of F_3dThd in plasma. F_3dThd in doses of 100 mg/kg were administered orally to wild-type and $TP^{-/-}$ mice. The mouse blood was collected at the indicated times and centrifuged to obtain plasma. The concentration of F_3dThd in plasma was measured as described previously (7).

Measurement of pentobarbital anesthetic effect. Five female wild-type, $TP^{-/-}$ and $TP^{-/-}$ $UP^{-/-}$ mice at 5 months of age were injected intraperitoneally with 50 or 55 mg of pentobarbital/kg of body weight. The time during which their postural reflex was lost was measured.

Effect of supplementation of the diet with high doses of thymidine. Five wild-type and $TP^{-/-}$ $UP^{-/-}$ mice at 3 months of age were fed 5 g of of thymidine/kg of body weight/day. Thymidine was mixed at a 1:30 (wt/wt) ratio with a CE-2 diet (CLEA Japan, Inc.). After a 7-month feeding period, the muscles, brain, and blood were removed and subjected to phenotype analysis.

Southern blot and PCR analysis of mtDNA. Total cellular DNA (8 to 10 μg) extracted from the muscles and brains of wild-type mice, $TP^{-/-}$ $UP^{-/-}$ mice, and high-dose thymidine-fed mice (wild-type and $TP^{-/-}$ $UP^{-/-}$ mice) was digested with the restriction enzyme (*Eco*RI) and Southern blotted as previously described (14). To measure the level of mtDNA in $TP^{-/-}$ $UP^{-/-}$ mice, the total cellular DNA (0.5 μg) was used as a template for the PCR analysis. The nucleotide sequences from positions 15495 to 15511 and from positions 15713 to 15697 were used as oligonucleotide primers (14).

Muscle biopsies. The soleus and extensor digitorum longus (EDL) muscle were obtained by dissection. A portion of the muscle specimens was immediately frozen in isopentane, cooled with liquid nitrogen, and then prepared for histochemical examination. Serial frozen sections were stained as described previously (10).

COX activity assays. COX activities were determined spectrophotometrically in postnuclear supernatants of fresh frozen muscle biopsy specimens as described previously (8). COX activity was expressed as nanomoles of ferrocytochrome *c* oxidized per minute per milligram of protein.

Determination of the concentration of lactic acid in plasma. The concentration of lactate in plasma from three mice at the age of 2 months was measured as described previously (27).

MRI and spectroscopy. Images were obtained on a UNITY-INOVA spectrometer (Varian, Palo Alto, Calif.) with a vertical 9.4-T magnet (Oxford, Oxford, United Kingdom). The mice were imaged at the age of 6 to 10 months under general anesthesia with 50 mg of pentobarbital sodium/kg. Three transverse fat-suppressed spin-echo images were obtained by using the following parameters: constant repetition time of 3 s and two averages; three different echo times (TE) of 10, 15, and 25 ms; field of view, 3 by 3 cm; matrix size, 256 by 128;

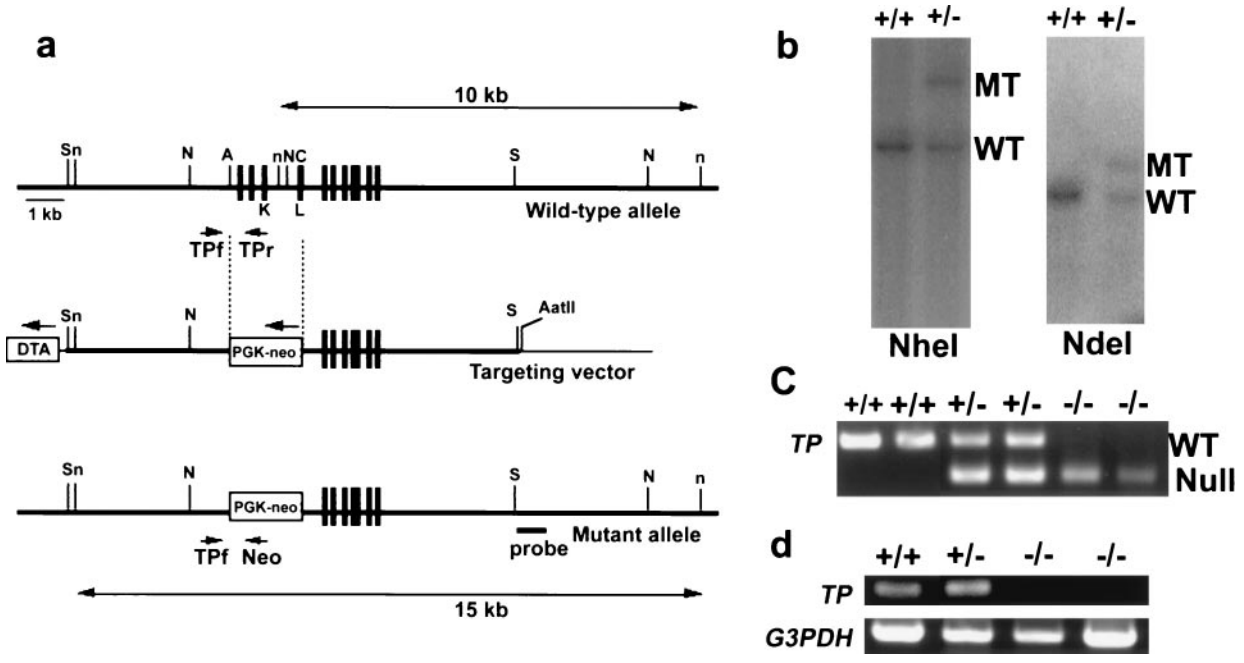

FIG. 1. Targeted disruption of the TP gene. (a) Schematic representation of the murine *TP* locus (top), the targeting vector (middle), and the mutated allele (bottom). The closed boxes denote the 10 exons of the *TP* gene. The targeting vector was designed to replace an exon encoding a portion of the phosphate- or deoxyribose-binding site (top [K or L]) with a neomycin resistance gene. The position of the 3′-flanking probe used for Southern blot analysis is indicated. Positions of the PCR primers for the wild-type allele (TPf and TPr) and the mutant allele (TPf and neo) are also shown. S, n, N, A, and C represent the *Spe*I, *Nhe*I, *Nde*I, *Afl*II, and *Cla*I sites, respectively. (b) Southern blot analysis of wild-type and mutant ES cell DNA. Genomic DNA from wild-type (+/+) and $TP^{+/-}$ (+/−) ES cell clones were digested with *Nhe*I (left) or *Nde*I (right) and hybridized with the 3′-flanking probe. The 10-kb wild-type fragment (WT) and the 15-kb mutant fragment (MT) obtained after *Nhe*I digestion are indicated on the left. The wild-type allele produced an 8.5-kb *Nde*I digestion product, whereas the mutant allele gave rise to an 11-kb hybridizing product (right). (c) PCR analysis of mouse tail DNA from the wild-type allele (+/+), heterozygous *TP*-null allele (+/−), and homozygous *TP*-null allele (−/−). Oligonucleotides TPf and TPr (see panel a) were used as primers for the upstream and downstream disruption sites, respectively. Oligonucleotides TPf and Neo were used as primers for the knockout allele. The amplified PCR products were analyzed on 1% agarose gels to separate the 640-bp wild-type (WT) and 400-bp *TP*-null (Null) targeted allele fragments. (d) Reverse transcription-PCR analysis of TP mRNA in the livers of wild-type mice (+/+), $TP^{+/-}$ (+/−) mice, and $TP^{-/-}$ (−/−) mice. The total RNA was isolated from the liver and reverse transcribed. The resulting cDNA was used for PCR analysis with specific primers for *TP* and for the murine glyceraldehyde-3-phosphate dehydrogenase (*G3PDH*) gene. A 300-bp band is amplified by the TP-specific primers (*TP*), and a 950-bp band represents mRNA for *G3PDH*.

and thickness, 1 mm. The data set was zero filled to 1024 by 1024 for reconstruction. Quantitative T_2 maps were created from the signal intensity of different TE images [S(TE)] fitted to a monoexponentially decaying function for each pixel in Imagebrowser software (Varian): $S(TE) = S_0 \exp(-TE/T_2)$.

Histological analysis of the brains. Whole brains from wild-type and $TP^{-/-}$ $UP^{-/-}$ mice were removed and immediately fixed in 1.5% paraformaldehyde–0.5% glutaraldehyde–phosphate-buffered saline and embedded in Epon. Toluidine blue-stained semithin sections were prepared, and sections were cut for electron microscopy on a transmission electron microscope (JEM-1200EX; JEOL, Ltd.)

RESULTS

In order to generate mice with a targeted deletion in the *TP* gene, a targeting vector was constructed in which the phosphate- or deoxyribose-binding site of TP was replaced with a neomycin resistance cassette. The targeting vector (Fig. 1a) was electroporated into ES cells, and colonies heterozygous for mutations in TP were detected by Southern blotting (Fig. 1b). Clones heterozygous for the targeted mutation were injected into C57BL/Swiss blastocytes to generate chimeric mice. The chimeras were crossed into C57BL/Swiss strains to produce heterozygous mutant mice. Intercrosses between $TP^{+/-}$ heterozygous mice generated $TP^{-/-}$ mice. Germ line transmission of the mutation was verified by PCR analysis of tail DNA (Fig. 1c). The null mutation of TP was confirmed by reverse transcription-PCR analysis of RNA extracted from mice livers (Fig. 1d). $TP^{-/-}$ mice were viable, survived to adulthood (at least 23 months after birth), were healthy and fertile, and were overtly normal in gross anatomy, tissue histology, and hematology (data not shown). In the progeny from $TP^{+/-}$ crosses, the distribution of $TP^{-/-}$ mice was consistent with Mendelian segregation (30 of 126). A thymidine analogue, F_3dThd, has been reported to be metabolized by TP and was therefore used to measure TP activity in the mutant and wild-type mice. F_3dThd (100 mg/kg) was administered orally to wild-type and $TP^{-/-}$ mice, and the concentration of F_3dThd in plasma was measured. F_3dThd levels in plasma from $TP^{-/-}$ mice were markedly increased (Fig. 2a), indicating that TP activity was decreased in these mice. We then measured the TP activities of various tissues from wild-type and $TP^{-/-}$ mice. Surprisingly, TP activity was impaired only in the livers of the $TP^{-/-}$ mice (Fig. 2b). We noted that another enzyme, UP, is capable of degrading thymidine in mice but not in humans. Thus, UP activity may be compensating for the absence of TP in the $TP^{-/-}$ mice. $UP^{-/-}$ mice have been generated by Tsujimoto et al. (23rd Annu. Meet. Mol. Biol. Soc. Japan, abstr. 1PB-204, p. 382, 2000).

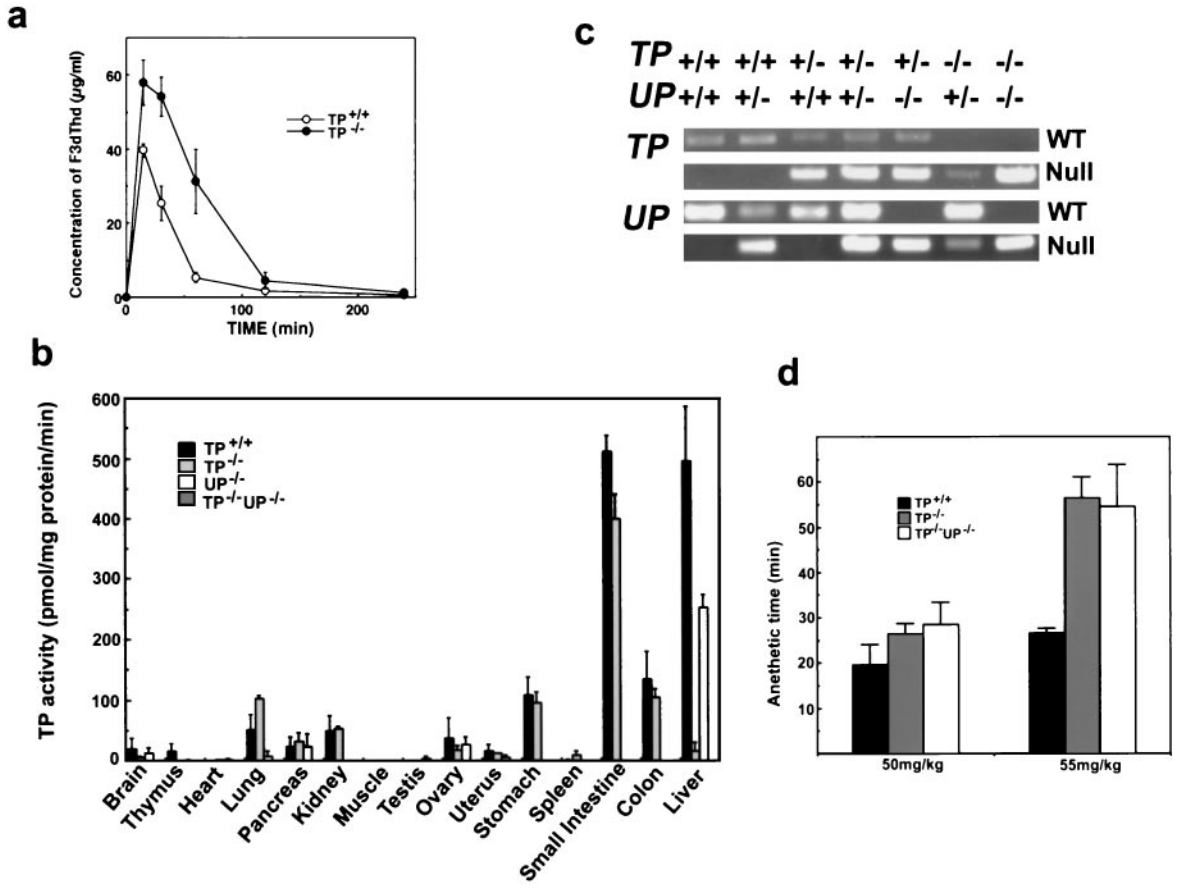

FIG. 2. Generation of mice with targeted deletions of both TP and UP. (a) Levels of F_3dThd in plasma in mice after administration of F_3dThd. F_3dThd (100 mg/kg) was administered orally to $TP^{+/+}$ and $TP^{-/-}$ mice. The concentration of F_3dThd in plasma was determined as described previously (7). Statistical significance was determined by using the Student's *t* test (mean ± the standard error; $n = 3$). (b) TP activity in various tissues from wild-type, $TP^{-/-}$, $UP^{-/-}$, and $TP^{-/-}$ $UP^{-/-}$ mice. The rate of conversion of thymidine to thymine was measured radiometrically as described previously (6). TP activity is expressed as nanomoles of thymidine catalyzed to thymine per minute per milligram of protein. Tissues were collected from three 2-month-old mice. (c) PCR analysis of mouse tail DNA from animals with the following six phenotypes: wild-type allele ($TP^{+/+}$ $UP^{+/+}$), heterozygous *TP*-null allele ($TP^{+/-}$ $UP^{+/+}$), homozygous *TP*-null allele ($TP^{-/-}$ $UP^{+/+}$), heterozygous *UP*-null allele ($TP^{+/+}$ $UP^{+/-}$), homozygous *UP*-null allele ($TP^{+/+}UP^{-/-}$), heterozygous *TP* or *UP* allele ($TP^{+/-}$ $UP^{+/-}$), and homozygous *TP*- and *UP*-null allele ($TP^{-/-}$ $UP^{-/-}$). The sizes of the amplified PCR products were 210 bp for UP wild type, 640 bp for TP wild type, 313 bp for the UP targeted allele, and 400 bp for the TP targeted allele fragments. (d) Five female mice at 5 months of age were injected intraperitoneally with pentobarbital. The time during which postural reflex was lost was measured.

These $UP^{-/-}$ mice survived for 2 years without losing weight. TP activities in most tissues of the $UP^{-/-}$ mice were almost inhibited, but the TP activity in the liver was retained (Fig. 2b). These data indicate that both TP and UP are involved in endogeneous thymidine metabolism and that targeted deletion of both the *TP* and the *UP* genes is required for inhibition of TP activity in mice.

We therefore generated $TP^{-/-}$ $UP^{-/-}$ mice by crossing $TP^{-/-}$ mice with $UP^{+/-}$ mice to generate $TP^{+/-}$ $UP^{+/-}$ mice, followed by intercrossing the mice to generate $TP^{-/-}$ $UP^{-/-}$ mice. Mice were genotyped routinely by PCR analysis of tail DNA (Fig. 2c). As expected, TP activities in the liver, small intestine, and other tissues were completely inhibited in $TP^{-/-}$ $UP^{-/-}$ mice (Fig. 2b). $TP^{-/-}$ $UP^{-/-}$ mice were viable, surviving for more than 16 months, and were fertile and overtly normal. This indicates that TP activity is dispensable for embryonic development and postnatal growth. However, the pentobarbital had a prolonged anesthetic effect on the $TP^{-/-}$ and $TP^{-/-}$ $UP^{-/-}$ mice compared to wild-type mice (Fig. 2d). In order to determine the relative contributions of TP and UP to thymidine metabolism, the levels of thymidine, uridine, and cytidine in the plasma of five mice at 5 weeks of age were also measured. Thymidine levels in plasma were >5-fold higher in $TP^{-/-}$ $UP^{-/-}$ mice compared to wild-type mice, whereas thymidine levels in the plasma of $TP^{-/-}$ mice were only 2-fold higher than those of wild-type mice (Fig. 3a). The thymidine level in the plasma of $UP^{-/-}$ mice was twofold higher than that of wild-type mice.

We then sought to determine whether $TP^{-/-}$ or $TP^{-/-}$ $UP^{-/-}$ mice could be used as a model for MNGIE disease in humans in which TP has been implicated as the causative gene. For this purpose, we examined whether the $TP^{-/-}$ or $TP^{-/-}$ $UP^{-/-}$ mice display the symptoms of MNGIE which have been reported in humans, i.e., muscle abnormalities, COX deficiency, cachexia, and lactic acidosis. Nishino et al. reported that COX-deficient fibers are identified in all MNGIE patients,

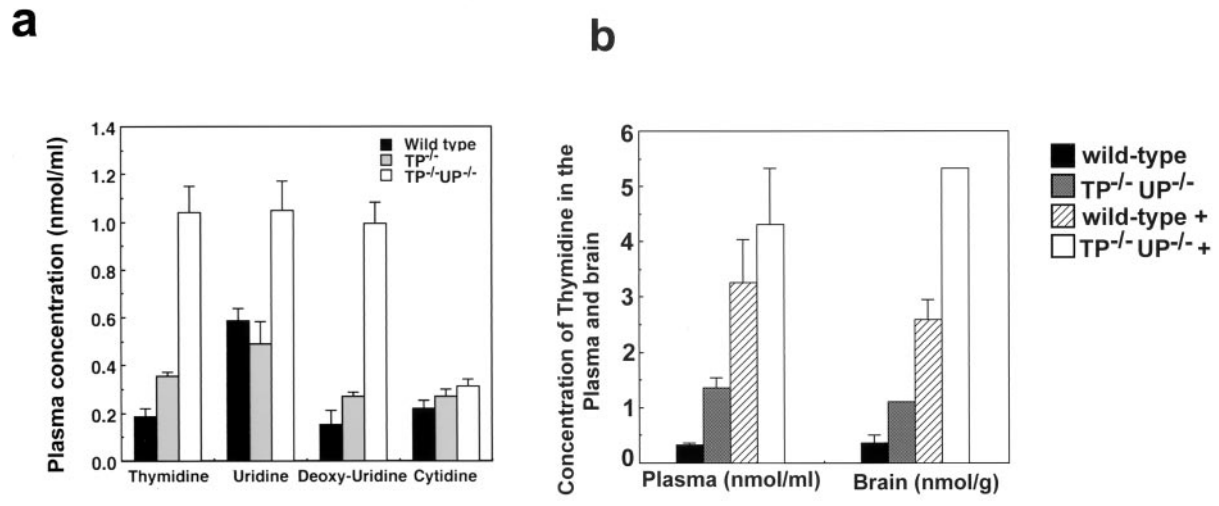

FIG. 3. Elevated concentrations of thymidine in the plasma and brains of $TP^{-/-}$ $UP^{-/-}$ mice. (a) Concentrations of pyrimidine nucleosides in the plasma of wild-type, $TP^{-/-}$, and $TP^{-/-}$ $UP^{-/-}$ mice. Blood was collected from five mice at the age of 2 months and centrifuged to obtain the plasma. An aliquot (0.2 ml) of mouse plasma was applied to a high-pressure liquid chromatography column. The concentrations of thymidine, uridine, and cytidine in plasma were then measured. (b) Concentrations of thymidine in the plasma and brains of wild-type mice, $TP^{-/-}$ $UP^{-/-}$ mice, and thymidine-fed mice (indicated as "wild-type+" and "$TP^{-/-}$ $UP^{-/-}$+").

and ragged-red fibers are seen in 63% of patients (22). We obtained the soleus and EDL muscles from age-matched wild-type, $TP^{-/-}$, and $TP^{-/-}$ $UP^{-/-}$ mice. A portion of the muscle specimens was immediately frozen and prepared for histochemical examination. Serial frozen sections were stained with modified Gomori trichrome (Fig. 4b, d, and f), hematoxylin and eosin (H&E), periodic acid-Schiff, and oil red O stains (data not shown). COX (Fig. 4a, c, and e), NADH-tetrazolium reductase, acid phosphatase, and succinate dehydrogenase were stained as described previously (10) (data not shown). We analyzed 12-month-old wild-type and $TP^{-/-}$ mice (Fig. 4a to d) and 10-month-old $TP^{-/-}$ $UP^{-/-}$ mice (Fig. 4e and f). We did not observe any morphological or histochemical differences in stained sections from the wild-type and $TP^{-/-}$ mice or from the $TP^{-/-}$ $UP^{-/-}$ mice. We did not observe ragged-red fibers in the sections stained with modified Gomori trichrome or in the sections stained for succinate dehydrogenase. We also detected a comparable COX activity in the wild-type, $TP^{-/-}$, and $TP^{-/-}$ $UP^{-/-}$ mice. (Fig. 4a, c, and e). We did not find any difference in COX activities of the cardiac muscle fibers from the wild-type and $TP^{-/-}$ $UP^{-/-}$ mice (data not shown). Since defects of mitochondrial respiratory chain enzymes are seen in 50% of MNGIE patients, we also spectrophotometrically determined the COX activities in postnuclear supernatants of fresh frozen muscle and liver tissues from wild-type, $TP^{-/-}$, and $TP^{-/-}$ $UP^{-/-}$ mice (Fig. 4i). We used 2-month-old mice, with three mice in each group. We did not observe any difference in COX activities among wild-type, $TP^{-/-}$, and $TP^{-/-}$ $UP^{-/-}$ mice (Fig. 4i). Cachexia is a prominent feature of MNGIE, and most patients are thin throughout their lives. To determine whether the body weight is altered in the $TP^{-/-}$ mice, we weighed the litters of the wild-type, $TP^{-/-}$, and $TP^{-/-}$ $UP^{-/-}$ mice every other week. The body weight curves were superimposable for each group (data not shown). Weight loss of $TP^{-/-}$ and $TP^{-/-}$ $UP^{-/-}$ mice has so far not been observed for 16 months of observation. Lactic acidosis is reported to be observed in 63% of MNGIE patients. The levels of lactic acid in plasma from $TP^{-/-}$ and $TP^{-/-}$ $UP^{-/-}$ mice were similar to those of wild-type mice (data not shown). The levels of thymidine in plasma are elevated nearly 20-fold in MNGIE patients (22), whereas thymidine levels in plasma were only fivefold higher in $TP^{-/-}$ UP $^{-/-}$ mice than in wild-type mice. We therefore fed wild-type and $TP^{-/-}$ $UP^{-/-}$ mice with thymidine (15 g/kg/day) for 7 months to increase the concentration of thymidine in the plasma and then examined whether these $TP^{-/-}$ $UP^{-/-}$ mice developed the symptoms of MNGIE. The thymidine level in plasma was elevated nearly 13-fold in these mice (Fig. 3b). Unexpectedly, we did not observe significant changes in stained sections from these mice. (Fig. 4a and g, b and h). Neither significant deletion nor depletion of mtDNA of the $TP^{-/-}$ $UP^{-/-}$ mice was detected (Fig. 4j).

Brain MRI revealed a striking leukoencephalopathy in all MNGIE patients. To determine whether a similar pathology was present in the $TP^{-/-}$ $UP^{-/-}$ mice, high-resolution in vivo imaging was performed on anesthetized mice (seven wild-type mice aged 8 to 12 months, six $TP^{-/-}$ $UP^{-/-}$ mice aged 6 to 9 months, and two $TP^{-/-}$ mice aged over 12 months) in a dedicated 9.4-T MRI scanner. High-intensity lesions on the T_2 map were seen in five of six brains from $TP^{-/-}$ $UP^{-/-}$ mice (Fig. 5b and c), in one of seven brains from wild-type mice (Fig. 5a), and in none of the brains of $TP^{-/-}$ mice (data not shown). We could not detect pathological changes in these lesions by H&E and KB staining. However, we noticed that enlarged myelinated fibers were conspicuous in the brains of $TP^{-/-}$ $UP^{-/-}$ mice (Fig. 5e and f) by toluidine blue staining. Although myelinated fibers of a similar caliber were also observed in the control mice, they were much more rare (Fig. 6d). Ultrastructural observation revealed that the myelin sheaths of the enlarged fibers in the $TP^{-/-}$ $UP^{-/-}$ mice have segmental

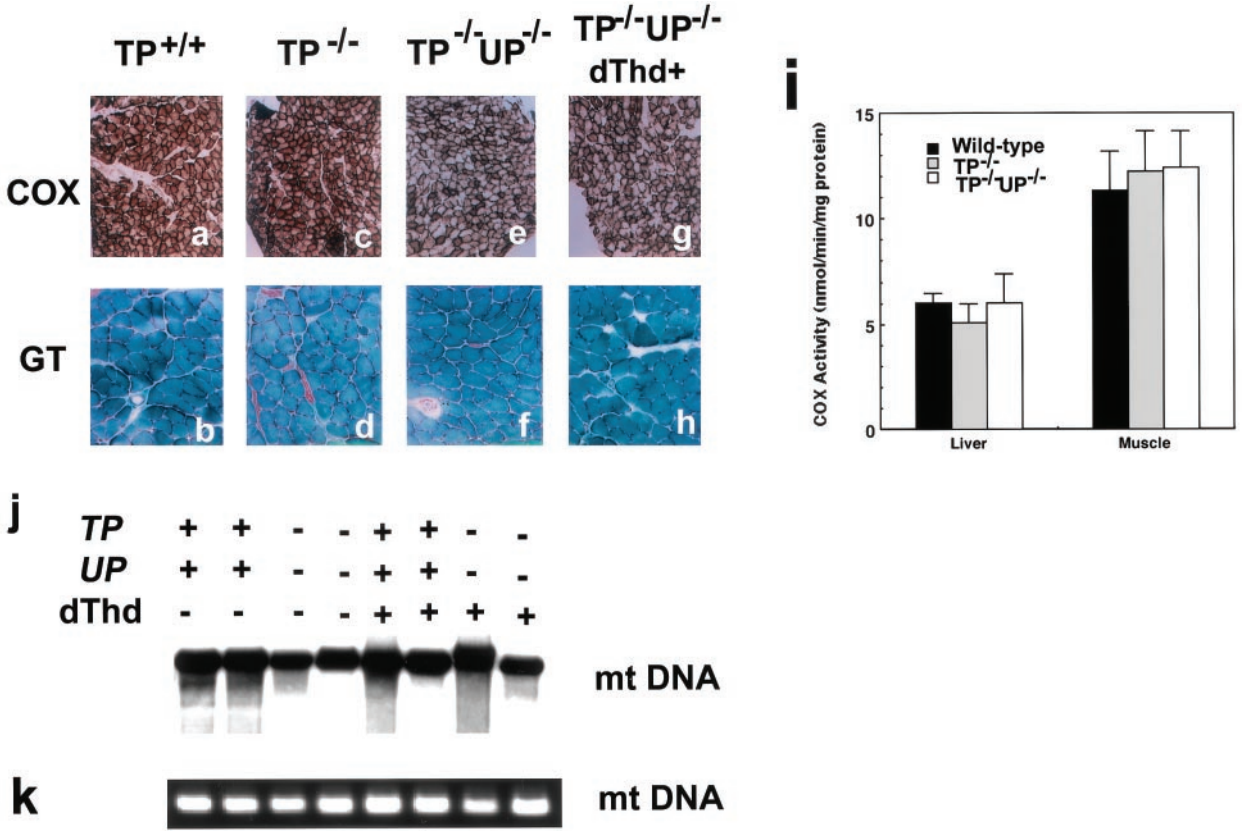

FIG. 4. Lack of significant features of MNGIE in the muscles of $TP^{-/-}$ $UP^{-/-}$ mice. The morphology of serial sections of muscles from 12-month-old wild-type ($TP^{+/+}$) mice (a and b) and $TP^{-/-}$ mice (c and d) and 10-month-old $TP^{-/-}$ $UP^{-/-}$ mice (e and f) and thymidine-fed $TP^{-/-}$ $UP^{-/-}$ mice (g and h) was examined. Histochemical staining of soleus muscle or EDL sections was done with modified Gomori trichrome (GT; shown in panels b, d, f, and h), and histochemical staining was done to detect COX (shown in panels a, c, e, and g). (i) COX activities in the lysates of leg muscles and livers from three 2-month-old wild-type and $TP^{-/-}$ mice were measured. (j and k) Southern blot (j) and PCR (k) analyses of mtDNA. The total DNAs from the muscles of wild-type mice (lanes 1 and 2), $TP^{-/-}$ $UP^{-/-}$ mice (lanes 3 and 4), and thymidine-fed (dThd+) mice (wild type, lanes 5 and 6; $TP^{-/-}$ $UP^{-/-}$, lanes 7 and 8) were tested to measure the amount of mtDNA.

dilatation in the tangential view and uneven protrusion in the transverse view (Fig. 6h and i). The ultrastructure of the axons was conserved, and such dilatation and protrusion were due to abnormal myelin structures. In contrast, these morphological changes were not observed in large caliber myelin sheaths in the wild-type mice (Fig. 6g). Meanwhile, we could not detect depletion of mtDNA in these brains (Fig. 5j, lanes 3 and 4). Thus, encephalopathy in MNGIE patients does not appear to be caused by mtDNA alteration. We therefore searched for other candidates that might be responsible for the clinical features of MNGIE in the muscles such as COX deficiency.

Since Nishino et al. reported that MNGIE is linked to chromosome 22q13.32, we carried out a careful examination of the genes located in this region. In the course of computer search, we found that the *TP* gene is located next to the *SCO2* (COX assembly protein isoform 2) gene, in which mutations have been reported in patients with fetal infantile cardioencephalomyopathy. We used the human *TP* cDNA sequence (GenBank accession no. NM_001953) and *Homo sapiens SCO* (cytochrome oxidase-deficient, yeast) homolog 2 (*SCO2*) mRNA (GenBank accession no. XM_017992) as queries in a human genome BLAST search against the working draft human genome sequence. The best matches were the chromosome 22 working draft sequence (GenBank accession no. HS22_11683) segment. The *SCO2* mRNA displayed 100% identity to the segment between positions 98997 and 100972, and the *TP* gene displayed 99% identity to the segment between positions 101181 and 105455 within the chromosome 22q13.33 region (Fig. 6a). We found the mouse *SCO2* homolog (GenBank accession no. AKO13765.1) by a BLAST (Blastn) search. The deduced amino acid sequence of AKO13765.1 also has the functionally conserved core region which is 89.9% identical to that of the human. Furthermore, AKO13765.1 has a CPDIC motif that binds two copper atoms (data not shown). Thus, we concluded that AKO13765.1 is a mouse homologue of the *SCO2* gene. Next, we examined the sequence homology between the mouse *TP* cDNA (GenBank accession no. AB06274) and the mouse *SCO2* gene. Exons 9 and 10 of the mouse *TP* gene showed 100% sequence identity to the mouse *SCO2* cDNA (Fig. 6b).

DISCUSSION

Loss of function of TP has been reported to cause MNGIE (20). As a consequence of the TP defect, the levels of thymidine in plasma are elevated. A high level of thymidine in plasma was assumed to impair mtDNA replication, repair, or both, leading to mtDNA abnormalities (21). mtDNA deletions are believed to be the predominant genetic abnormal-

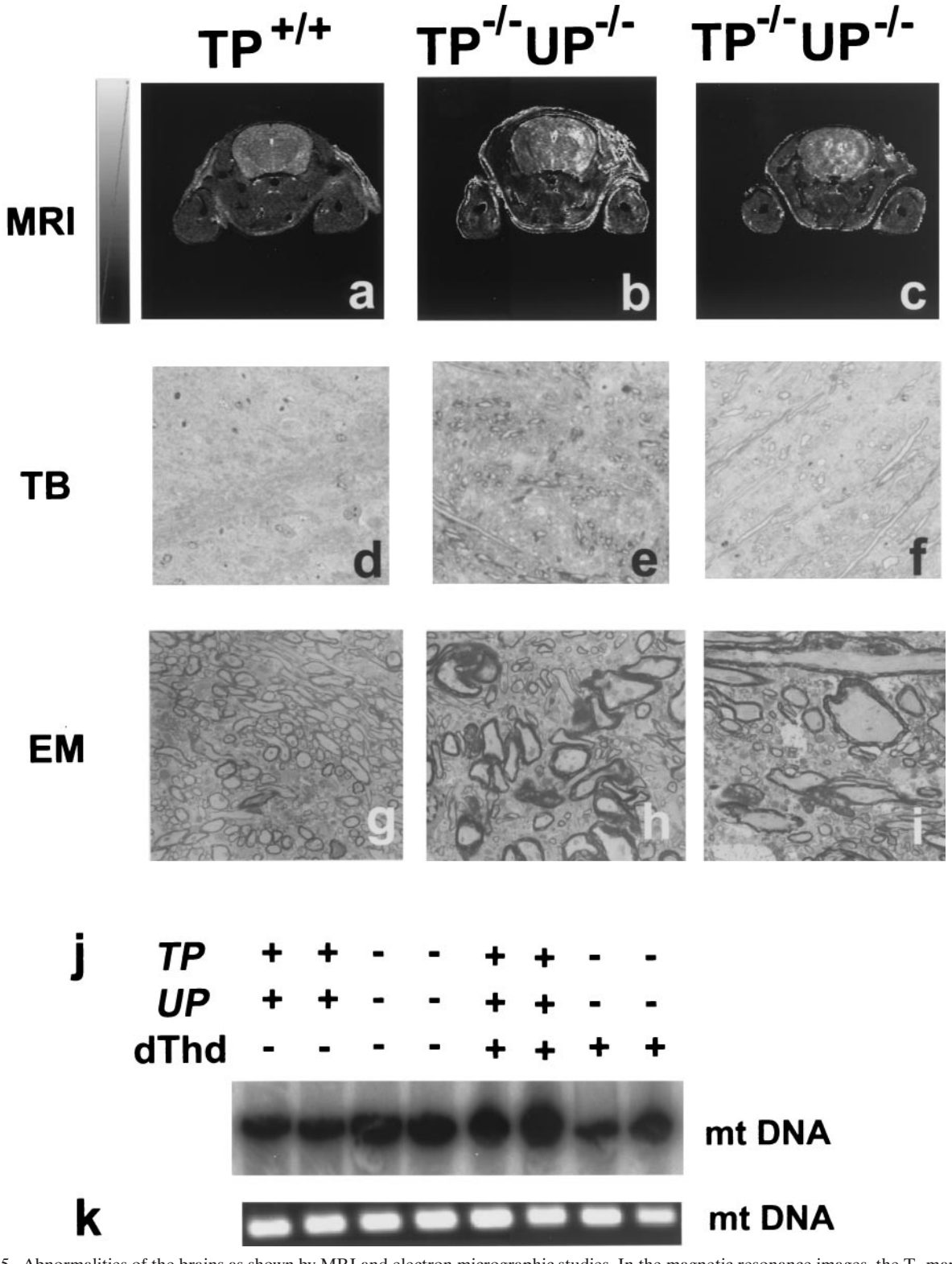

FIG. 5. Abnormalities of the brains as shown by MRI and electron micrographic studies. In the magnetic resonance images, the T_2 maps at 9.4 T at the level of lateral ventricles in wild-type (a) and $TP^{-/-}$ $UP^{-/-}$ (b and c) mice are shown. The gray scale for T_2 maps ranges from 0 to 80 ms. (d to f) Light microscopic sections of the brains from the wild-type and $TP^{-/-}$ $UP^{-/-}$ mice brain were examined by toluidine blue (TB) staining. (g to i) Ultrastructures of myelinated fibers as viewed by electron microscopy (EM). The enlarged myelinated fibers were conspicuous in $TP^{-/-}$ $UP^{-/-}$ mouse brains (see panels e, f, h, and i). Magnification, ×2,000. (j and k) Southern blot (j) and PCR (k) analyses of mtDNA. The total DNAs from the muscles of wild-type mice (lanes 1 and 2), $TP^{-/-}$ $UP^{-/-}$ mice (lanes 3 and 4), and thymidine-fed ($dThd^{+}$) mice (wild type, lanes 5 and 6; $TP^{-/-}$ $UP^{-/-}$, lanes 7 and 8) were tested to measure the amount of mtDNA.

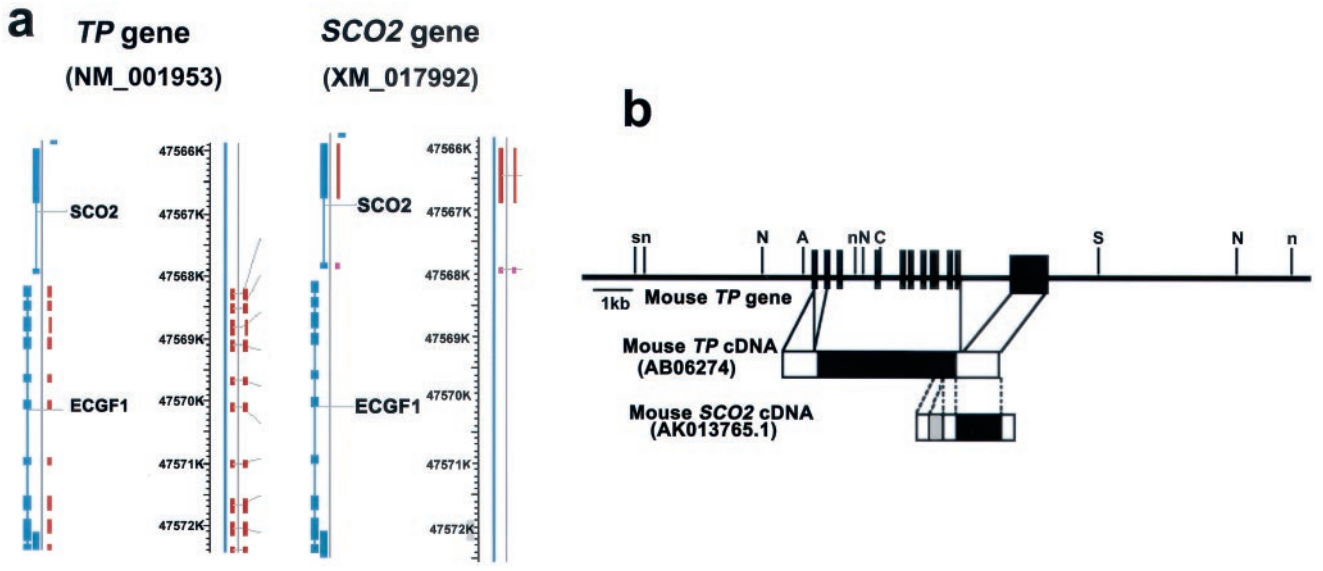

FIG. 6. The *TP* gene overlaps with the *SCO2* gene. (a) Chromosomal positions of the human *TP* (NM_001953) and human *SCO2* (XM_017992) genes. The best match of these genes determined by a BLAST search against the human genome sequence was a chromosome 22 working draft sequence segment (HS22_11683). The *TP* gene lies between positions 45508430 and 45504150, and the *SCO2* gene lies between positions 45503950 and 45501950 within chromosome 22q13.33. (b) Schematic diagram of the mouse *TP* and *SCO2* gene structures. Schematic representation of the murine *TP* gene (top), *TP* cDNA (middle), and murine *SCO2* cDNA (bottom). The coding regions of both cDNAs are shown as black boxes, and noncoding regions are shown as white boxes. The cDNA sequence of *SCO2* shares exons 9 and 10 of *TP*, indicated as white boxes (noncoding region) and a black box (coding region). In addition to these sequences, *SCO2* cDNA has a unique sequence in the 5′-noncoding region as indicated by a gray box.

ity associated with MNGIE (24). To explore the effect of TP on the MNGIE phenotype, we generated $TP^{-/-}$ mice. Unexpectedly, these mice appear overtly normal and do not show any clinical or biochemical features of MNGIE. Although the oldest litters are 23 months old, they appear normal. However, TP activities in $TP^{-/-}$ mice were not completely inhibited. We noted that mouse UP also cleaves thymidine (5), and thus UP may contribute to TP activity in the mouse. This was confirmed by measurement of TP activity in $UP^{-/-}$ mice. In these mice TP activity was reduced in most tissues except in the liver. These data suggested that metabolism of thymidine in the liver is regulated mainly by TP but that in other tissues it is regulated mainly by UP. We therefore generated $TP^{-/-}$ $UP^{-/-}$ mice in order to fully inhibit mouse TP activities. Although our study did not demonstrate the clinical symptoms of MNGIE, MR T_2 maps of the brains of $TP^{-/-}$ $UP^{-/-}$ mice revealed hyperintense lesions that could be the first clue to the histological basis of this disease. Ultrastructural observation revealed that the myelin sheaths of the enlarged fibers in the $TP^{-/-}$ $UP^{-/-}$ mice have segmental dilatation in the tangential view and uneven protrusion in the transverse view. The ultrastructure of the axons was conserved, and such dilatation and protrusion were due to abnormal myelin structures. We were unable to find macrophages that contain myelin debris, which indicated that complete disruption of the myelin sheaths did not take place in the $TP^{-/-}$ $UP^{-/-}$ mice brain. Thus, the specific ultrastructural changes of the myelin sheaths were considered to restore without leaving residual pathology. This observation could explain the fact that $TP^{-/-}$ $UP^{-/-}$ mice show abnormal nuclear magnetic resonance images without detectable neurological abnormalities. The histological basis of the MRI findings in MNGIE patients has not been elucidated because live brain biopsies cannot be done in humans. Thus, it is still unclear that this edematization of mouse brains is exactly the same as the leukoencephalopathy in MNGIE patients. However, this is the first mouse model which may provide further insights into the histological basis of the hyperintense MRI abnormality. Pathological features of MNGIE have not been observed in the muscles of $TP^{-/-}$ $UP^{-/-}$ mice for up to 16 months after birth even though the mice were fed with thymidine (15 g/kg/day) for 7 months to increase the concentration of thymidine in plasma. Although the thymidine levels in the plasma were >13-fold higher than in the control mouse and the thymidine levels in plasma in normal mice were reportedly 10-fold higher than in humans, mtDNA alterations were not detected in either the brains or the muscles of these $TP^{-/-}$ $UP^{-/-}$ mice. The large variation in the age of onset of MNGIE, which ranges from 5 months to 43 years (24) in spite of the negligible TP activity and high levels of thymidine in plasma in most of the patients, suggests that the loss-of-function mutation in the *TP* gene may not be sufficient to cause MNGIE. Thus, other gene(s) besides *TP* gene might be involved in the incidence of MNGIE. One potential candidate gene is *SCO2*. Exon 10 of the human *TP* gene is positioned next to the *SCO2* gene. Mutations in *SCO2* have recently been reported to cause severe COX deficiency in skeletal muscle leading to mitochondrial disorders characterized by hypertrophic cardiomyopathy and encephalopathy. Since *TP* was identified as a potential causative gene for MNGIE in a genetic linkage study (20), it is possible that

genes adjacent to or overlapping the *TP* gene, such as *SCO2*, can contribute to the disease. A second gene which may be involved in causing the clinical symptoms of MNGIE is thymidine kinase 2 (TK2) as delineated in a model proposed by Wang and Eriksson (36). TK2 exists in mitochondria and in phosphorylate thymidine, 2′-deoxyuridine, and deoxycytidine. Unlike thymidine kinase 1 (TK1), TK2 is expressed not only in growing cells but also in terminally differentiated cells. Thus, in nonproliferating tissues such as muscles, TK2 is the only pyrimidine nucleoside salvage enzyme and may play an important role in mtDNA replication. Therefore, TK2 activity, as well as the inhibition of TP activity, may be needed for the incidence of MNGIE. Since depletion in the mtDNA was not detected in $TP^{-/-}$ $UP^{-/-}$ mice, TK2 activity in $TP^{-/-}$ $UP^{-/-}$ mice may be different from that in MNGIE patients. An alternative explanation for the lack of mitochondrial pathology in the $TP^{-/-}$ $UP^{-/-}$ mice is that a high dose of thymidine may not impair mtDNA replication or repair in mouse cells even though it does so in human cells (14). It is still unclear whether a high level of thymidine in plasma actually impairs muscle mtDNA or how much mtDNA alterations contribute to the pathology of MNGIE. MNGIE patients with no mtDNA alterations detectable by Southern blot or PCR analyses have been reported by Hamano et al. (9). The patients fulfilled the diagnostic clinical and pathological criteria of MNGIE proposed by Hirano et al., including leukoencephalopathy on brain MRI. In two other reports, mtDNA abnormalities were not observed in 5 of 13 and 4 of 8 MNGIE patients, respectively (3, 13). Our findings are consistent with these studies and indicate that the inhibition of TP activity causes elevation of pyrimidine levels in plasma and axonal swelling in the brains of mice but does not cause abnormalities of mtDNA. Further study is needed to determine the causal relationship between the incidence of axonal swelling and the elevated thymidine level in plasma. The lack of TP activity in the livers of some MNGIE patients may have implications for therapy of this disease. $TP^{-/-}$ and $TP^{-/-}$ $UP^{-/-}$ mice had serious delays compared to normal mice in their recovery from anesthetization and also showed altered pharmacokinetics of the antimetabolites. Pentobarbital is reported to be degraded in the liver (29). The defect of TP activity in the liver may be associated with the prolonged anesthetic effect of pentobarbital in the $TP^{-/-}$ and $TP^{-/-}$ $UP^{-/-}$ mice. The role of TP in the detoxification of thymidine analogs should be taken into account when treating MNGIE patients. Thus, since the thymidine analogue F_3dThd is metabolized and detoxified by TP, lower concentrations of this thymidine analogue should be given to MNGIE patients who have lost TP activity. Conversely, some prodrugs such as 5′-deoxy-5-fluoridine that are activated by TP would presumably not be effective in MNGIE patients lacking TP activity. The $TP^{-/-}$ $UP^{-/-}$ mouse model that we have developed will be a useful tool to elucidate the physical roles of TP activity and to analyze the correlation between pathogenesis of MNGIE and aberrant thymidine metabolism and will provide information necessary for the effective and safe treatment of MNGIE patients. Most importantly, it is the first mouse model which may allow dissection of the histological basis of the brain abnormalities in this disease.

ACKNOWLEDGMENTS

We gratefully acknowledge R. Wesselshmidt (Genomesystems, Inc.) for culture of the ES cells and production of the chimeric mice. We also thank E. Sudo for the mice breeding and the PCR analyses; N. Hirata, T. Kodama, and N. Misawa for histological analysis; and G. Yamada, A. Aiba, M. Nakagawa, and H. Yamamoto for insightful comments. We thank S. Narisawa for many helpful suggestions.

This work was supported in part by a grant-in-aid from the Ministry of Education, Culture, Sports, Science, and Technology of Japan.

REFERENCES

1. **Brown, N. S., and R. Bicknell.** 1998. Thymidine phosphorylase, 2-deoxy-D-ribose and angiogenesis. Biochem. J. **334**(Pt. 1)**:**1–8.
2. **Carrozzo, R., M. Hirano, B. Fromenty, C. Casali, F. M. Santorelli, E. Bonilla, S. DiMauro, E. A. Schon, and A. F. Miranda.** 1998. Multiple mtDNA deletions features in autosomal dominant and recessive diseases suggest distinct pathogeneses. Neurology **50:**99–106.
3. **Debouverie, M., M. Wagner, X. Ducrocq, Y. Grignon, B. Mousson, and M. Weber.** 1997. MNGIE syndrome in two siblings. Rev. Neurol. **153:**547–553.
4. **Dickinson, E. K., D. L. Adams, E. A. Schon, and D. M. Glerum.** 2000. A human SCO2 mutation helps define the role of Sco1p in the cytochrome oxidase assembly pathway. J. Biol. Chem. **275:**26780–26785.
5. **elKouni, M. H., M. M. elKouni, and F. N. Naguib.** 1993. Differences in activities and substrate specificity of human and murine pyrimidine nucleoside phosphorylases: implications for chemotherapy with 5-fluoropyrimidines. Cancer Res. **53:**3687–3693.
6. **Eng-Gan, T., L. Hallman, G. R. Pilkington, and M. B. van der Weyden.** 1981. A rapid and simple radiometric assay for thymidine phosphorylase of human peripheral blood cells. Clin. Chim. Acta **116:**237–243.
7. **Fukushima, M., N. Suzuki, T. Emura, S. Yano, H. Kazuno, Y. Tada, Y. Yamada, and T. Asao.** 2000. Structure and activity of specific inhibitors of thymidine phosphorylase to potentiate the function of antitumor 2′-deoxyribonucleosides. Biochem. Pharmacol. **59**:1227–1236.
8. **Glerum, M., B. H. Robinson, C. Spratt, J. Wilson, and D. Patrick.** 1987. Abnormal kinetic behavior of cytochrome oxidase in a case of Leigh disease. Am. J. Hum. Genet. **41:**584–593.
9. **Hamano, H. T., Ohta, Y. Takekawa, K. Kouda, and Y. Shinohara.** 1997. Mitochondrial neurogastrointestinal encephalomyopathy presenting with protein losing gastroenteropathy and serum copper deficiency. Rinsho Shinkeigaku **37:**917–922.
10. **Higuchi, I., K. Takahashi, S. Nakahara, M. Izumo, M. Nakagawa, and M. Osame.** 1991. Experimental germanium myopathy. Acta Neuropathol. **82:**55–59.
11. **Hirano, M., J. de Yebenes Garcia, A. C. Jones, I. Nishino, S. DiMauro, J. R. Carlo, A. N. Bender, A. F. Hahn, L. M. Salberg, D. E. Weeks, and T. G. Nygaard.** 1998. Mitochondrial neurogastrointestinal encephalomyopathy syndrome maps to chromosome 22q13.32-qter. Am. J. Hum. Genet. **63:**526–533.
12. **Hirano, M., and T. H. Vu.** 2000. Defects of intergenomic communication: where do we stand? Brain Pathol. **10:**451–461.
13. **Hirano, M., G. Silvestri, D. M. Blake, A. Lombes, C. Minetti, E. Bonilla, A. P. Hays, R. E. Lovelace, I. Butler, and T. E. Bertorini.** 1994. Mitochondrial neurogastrointestinal encephalopathy (MNGIE): clinical, biochemical, and genetic features of an autosomal recessive mitochondrial disorder. Neurology **44:**721–727.
14. **Inoue, K., S. Ito, D. Takai, A. Soejima, H. Shisa, J. B. LePecq, E. Segal-Bendirdjian, Y. Kagawa, and J. Hayashi.** 1997. Isolation of mitochondrial DNA-less mouse cell lines and their application for trapping mouse synaptosomal mitochondrial DNA with deletion mutations. J. Biol. Chem. **272:**15510–15515.
15. **Ishikawa, F., K. Miyazono, U. Hellman, H. Drexler, C. Wernstedt, K. Hagiwara, K. Usuki, F. Takaku, W. Risau, and C. H. Heldin.** 1989. Identification of angiogenic activity and the cloning and expression of platelet-derived endothelial cell growth factor. Nature **338:**557–562.
16. **Jaksch, M., I. Ogilvie, J. Yao, G. Kortenhaus, H. G. Bresser, K. D. Gerbitz, and E. A. Shoubridge.** 2000. Mutations in SCO2 are associated with a distinct form of hypertrophic cardiomyopathy and cytochrome *c* oxidase deficiency. Hum. Mol. Genet. **9:**795–801.
17. **Miyadera, K., T. Sumizawa, M. Haraguchi, H. Yoshida, W. Konstanty, Y. Yamada, and S. Akiyama.** 1995. Role of thymidine phosphorylase activity in the angiogenic effect of platelet derived endothelial cell growth factor/thymidine phosphorylase. Cancer Res. **55:**1687–1690.
18. **Moghaddam, A., and R. Bicknell.** 1992. Expression of platelet-derived endothelial cell growth factor in *Escherichia coli* and confirmation of its thymidine phosphorylase activity. Biochemistry **31:**12141–12146.
19. **Moghaddam, A., H. T. Zhang, T. P. Fan, D. E. Hu, V. C. Lees, H. Turley, S. B. Fox, K. C. Gatter, A. L. Harris, and R. Bicknell.** 1995. Thymidine phosphorylase is angiogenic and promotes tumor growth. Proc. Natl. Acad. Sci. USA **92:**998–1002.
20. **Nishino, I., A. Spinazzola, and M. Hirano.** 1999. Thymidine phosphorylase

gene mutations in MNGIE, a human mitochondrial disorder. Science **283:** 689–692.
21. **Nishino, I., A. Spinazzola, A. Papadimitriou, S. Hammans, I. Steiner, C. D. Hahn, A. M. Connolly, A. Verloes, J. Guimaraes, I. Maillard, H. Hamano, M. A. Donati, C. E. Semrad, J. A. Russell, A. L. Andreu, G. M. Hadjigeorgiou, T. H. Vu, S. Tadesse, T. G. Nygaard, I. Nonaka, I. Hirano, E. Bonilla, L. P. Rowland, S. DiMauro, and M. Hirano.** 2000. Mitochondrial neurogastrointestinal encephalomyopathy: an autosomal recessive disorder due to thymidine phosphorylase mutations. Ann. Neurol. **47:**792–800.
22. **Nishino, I., A. Spinazzola, and M. Hirano.** 2001. MNGIE: from nuclear DNA to mitochondrial DNA. Neuromusc. Disorders **11:**7–10.
23. **O'Brien, T., D. Cranston, S. Fuggle, R. Bicknell, and A. L. Harris.** 1995. Different angiogenic pathways characterize superficial and invasive bladder cancer. Cancer Res. **55:**510–513.
24. **Papadimitriou, A., G. P. Com, G. M. Hadjigeorgiou, A. Bordoni, M. Sciacco, L. Napoli, A. Prelle, M. Moggio, G. Fagiolari, N. Bresolin, S. Salani, I. Anastasopoulos, G. Giassakis, R. Divari, and G. Scarlato.** 1998. Partial depletion and multiple deletions of muscle mtDNA in familial MNGIE syndrome. Neurology **51:**1086–1092.
25. **Papadopoulou, L. C., C. M. Sue, M. M. Davidson, K. Tanji, I. Nishino, J. E. Sadlock, S. Krishna, W. Walker, J. Selby, D. M. Glerum, R. V. Coster, G. Lyon, E. Scalais, R. Lebel, P. Kaplan, S. Shanske, D. C. De Vivo, E. Bonilla, M. Hirano, S. DiMauro, and E. A. Schon.** 1999. Fatal infantile cardioencephalomyopathy with COX deficiency and mutations in SCO2, a COX assembly gene. Nat. Genet. **23:**333–337.
26. **Pauly, J. L., M. G. Schuller, and A. A. Zelcer.** 1977. Identification and comparative analysis of thymidine phosphorylase in the plasma and ascites fluids of tumor-bearing animals. J. Natl. Cancer Inst. **58:**1587–1590.
27. **Robinson, B. H., J. Ward, P. Goodyer, and A. Baudet.** 1986. Respiratory chain defects in the mitochondria of cultured skin fibroblast from three patients with lactic acidemia. J. Clin. Investig. **77:**1422–1427.
28. **Shimaoka, S., S. Matsushita, T. Nitanda, A. Matsuda, T. Nioh, T. Suenaga, Y. Nishimata, S. Akiba, S. Akiyama, and H. Nishimata.** 2000. The role of thymidine phosphorylase expression in the invasiveness of gastric carcinoma. Cancer **88:**2220–2227.
29. **Stella, V. J., and C. K. Chu.** 1980. Effect of short-term exposure to polychlorinated biphenyls on first-pass metabolism of pentobarbital in rats. J. Pharm. Sci. **69:**1279–1282.
30. **Stevenson, D. P., S. R. Milligan, and W. P. Collins.** 1998. Effects of platelet-derived endothelial cell growth factor/thymidine phosphorylase, substrate, and products in a three-dimensional model of angiogenesis. Am. J. Pathol. **152:**1641–1646.
31. **Sue, C. M., C. Karadimas, N. Checcarelli, K. Tanji, L. C. Papadopoulou, F. Pallotti, F. L. Guo, S. Shanske, M. Hirano, D. C. De Vivo, R. van Coster, P. Kaplan, E. Bonilla, and S. DiMauro.** 2000. Differential features of patients with mutations in two COX assembly genes, SURF-1 and SCO2. Ann. Neurol. **47:**589–595.
32. **Sumizawa, T., T. Furukawa, M. Haraguchi, A. Yoshimura, A. Takeyasu, M. Ishizawa, Y. Yamada, and S. Akiyama.** 1993. Thymidine phosphorylase activity associated with platelet-derived endothelial cell growth factor. J. Biochem. **114:**9–14.
33. **Takebayashi, Y., K. Yamada, K. Miyadera, T. Sumizawa, T. Furukawa, F. Kinoshita, D. Aoki, H. Okumura, Y. Yamada, S. Akiyama, and T. Aikou.** 1996. The activity and expression of thymidine phosphorylase in human solid tumours. Eur. J. Cancer **32A:**1227–1232.
34. **Takebayashi, Y., S. Akiyama, S. Akiba, K. Yamada, K. Miyadera, T. Sumizawa, Y. Yamada, F. Murata, and T. Aikou.** 1996. Clinicopathologic and prognostic significance of an angiogenic factor, thymidine phosphorylase, in human colorectal carcinoma. J. Natl. Cancer Inst. **88:**1110–1117.
35. **Usuki, K., J. Saras, J. Waltenberger, K. Miyazono, G. Pierce, A. Thomason, and C. H. Heldin.** 1992. Platelet-derived endothelial cell growth factor has thymidine phosphorylase activity. Biochem. Biophys. Res. Commun. **184:** 1311–1316.
36. **Wang, L., and S. Eriksson.** 2000. Cloning and characterization of full-length mouse thymidine kinase 2: the N-terminal sequence directs import of the precursor protein into mitochondria. Biochem. J. **351:**2469–2476.
37. **Yoshimura, A., Y. Kuwazuru, T. Furukawa, H. Yoshida, K. Yamada, and S. Akiyama.** 1990. Purification and tissue distribution of human thymidine phosphorylase: high expression in lymphocytes, reticulocytes and tumors. Biochim. Biophys. Acta **1034:**107–113.